Sixth International Symposium on Turbulence and Shear Flow Phenomena
Seoul, Korea, 22-24 June 2009

TURBULENCE SIMULATION FOR BEDLOAD SEDIMENT TRANSPORT

H.V. Truong, J.C. Wells
Department of Civil and Environmental Engineering,
Ritsumeikan University
Noji Higashi 1-1-1, Kusatsu, Shiga 525-8577, Japan
truongvuhung@yahoo.com, jwells@se.ritsumei.ac.jp

Grétar Tryggvason
Department of Mechanical Engineering
Worcester Polytechnic Institute
100 Institute Rd, Worcester, Massachusetts 01609-2280
gretar@wpi.edu

ABSTRACT

In "bedload transport", sediment particles are driven in a thin layer near the sediment bed by a (normally) turbulent flow, thereby shaping rivers and the seacoast. Herein, we present a fictitious-domain method for numerical simulation of the dense-phase motion of solid particles in turbulent liquid, possibly including a free liquid-gas surface, and apply it to bedload sediment transport in rotating drum flows and in minimal channel flow with a stress-free lid.

To accelerate progress in understanding and modelling of bedload transport, we aim to perform "quasi-direct" numerical simulation that resolves all stress-supporting eddies, *i.e.* at least down to the scale of particle diameter. For computatational tractability, we employ the "fictitious domain" technique wherein a standard incompressible Navier-Stokes solver is applied on a fixed uniform Cartesian grid. In the present implementations, the grid density allows at least four points per particle diameter. A *variable-density* solver is modified to recover rigid body motion inside particles by adding body forces to the governing equation. The resolution should capture, though roughly, the eddies mentioned above, but is not sufficient to resolve boundary layers around particles.

We compare computational results with experimental data from rotating drums, including a new "open-perimeter" drum that permits a free-surface flow over the particle bed. Overall agreement between experimental and simulated values of bed and free-surface angles is satisfactory. We then present data from simulations of bedload transport in a doubly-periodic "minimal channel" with a nominal friction Reynolds number of 250, and 40 grid points in the vertical and span directions. Though under-resolved, we believe these are the first reported simulations of bedload transport that are "quasi-DNS" in the sense that they resolve the particle-scale turbulence.

WHY QUASI-D.N.S. OF BEDLOAD TRANSPORT ?

Sediment transport shapes riverbeds and seabeds. "Bedforms" such as dunes and ripples often result, thus raising flow resistance and increasing flood levels. Our work focuses on the thin layer of mobile sediment near the bed called the "bedload layer", which physically entails the difficulties of turbulent two-phase shear flow, as "overlayed" upon plastic behavior of the sediment bed (cf. results section).

In view of the experience with single-phase wall turbulence - a far cleaner subject - we have concluded that further progress on bedload transport demands little less than Direct Numerical Simulation (DNS) of the near-bed phenomena. To resolve the complex motion of particles in bedload transport requires tracking 3D particles individually (e.g. Werner & Haff, 1988; Schmeeckle, 1998; Gotoh et al. 2000; Drake & Calantoni, 2001). Further, given the absence of reliable turbulence models for concentrated two-phase flow, one should resolve all stress-supporting scales of the turbulence. Similarly, the instantaneous local flow around particles should be resolved, as point models of fluid force are completely invalid in the present context.

Even in a "minimal channel", however, true DNS of bedload transport remains beyond the reach of practically available computers. To lower computational cost, we apply the "fictitious domain" technique; a standard incompressible, variable-density Navier-Stokes solver is applied on a fixed uniform Cartesian grid. The solver is modified to recover rigid body motion inside particles by adding body forces to the governing equation. Herein, a grid density of at least four points per particle diameter is employed; this should suffice to resolve the particle-scale eddies evoked above, though not the particles' boundary layers. We accordingly refer to these simulations as "quasi-DNS". No subgrid-scale turbulence model is currently employed, though it is likely that one would be advisable in some foreseeable applications.

After presenting the computational scheme, this paper first reviews some experimental checks, namely a rotating tumbler partially-filled with spherical particles in both a closed configuration (Truong et al. 2006), and a novel "open" design (Truong et al. 2007b). The latter employs externally circulating oil to maintain a free-surface flow inside the rotating tumbler, and the particle flow is now driven by a turbulent shear flow, rather than by the immersed weight of the particles. It can thus be considered a form of "bedload transport".

Next, we present results from computations of bedload transport in a doubly-periodic computational domain. The simulations are clearly under-resolved, and in this regard do not compare favorably with better resolved treatments, e.g. the simulations of near-threshold bedload motion by Uhlmann (2006). We believe however that presenting results at this resolution will help to identify the pacing issues that face achievement of "acceptable" reliability for transport at *moderate to high sediment flux*, and indeed to make hypotheses about the important physics. Note that serious engineering predictions of sediment flux under combined waves and currents can vary more than a hundredfold depending on the formula employed. Accordingly, "acceptable" accuracy could mean a factor of two. By this admittedly loose criterion, we

claim to have achieved the first reported simulations of bed-load transport at non-vanishing sediment flux that qualify as "quasi-DNS", inasmuch as they are 3D and resolve turbulent structure at the scale of the particle diameter.

FICTITIOUS-DOMAIN ALGORITHM

In the fictitious-domain method, the solid and liquid phases are handled together by a common Navier-Stokes solver on a Cartesian grid. To satisfy the required conditions on and within solid surfaces, an artificial body force $\boldsymbol{f}_p$ is added:

$$\frac{D(\rho \boldsymbol{u})}{Dt} = \nabla.(\boldsymbol{p} + \mu[\nabla \boldsymbol{u} + (\nabla \boldsymbol{u})^T]) + \rho \boldsymbol{g} + \boldsymbol{f}_p \qquad (1)$$

$$\nabla \cdot \boldsymbol{u} = 0 \qquad (2)$$

In the present work, $\boldsymbol{f}_p$ redistributes (angular) momentum within free particles to recover rigid motion therein.

Particle- fluid interaction

Within the fictitious domain framework, Kajishima & Takiguchi (2002) have proposed to simply force the velocity field to recover rigid motion within particles, in proportion to the solid volume fraction α in a given momentum cell

$$\boldsymbol{f}_p(\boldsymbol{x}) = \alpha\rho \frac{(\boldsymbol{u}_p(\boldsymbol{x}) - \boldsymbol{u}(\boldsymbol{x}))}{\Delta t} \qquad (3)$$

where $\boldsymbol{u}$ is the partial-step velocity in a grid cell, and $\boldsymbol{u}_p = \boldsymbol{U}_p + \bar{\Omega}_p \times \boldsymbol{r}$ is the particle's target velocity at the grid cell. This efficient algorithm has permitted calculating the motion of 1000 or more solid particles in a turbulent flow, with particle Reynolds number in the range 10˜300. Subsequent work (Uhlmann 2005; Truong et al. 2005a) has shown that forcing at Lagrangian "markers"at the particle surface and within the particle achieves greater accuracy, but at a significant cost in computational time. Accordingly, Truong et al. (2005b) have combined marker and volumetric forcing; the former is applied at particle surfaces, the latter within particles. In this way, the no-slip condition at particle surfaces is better satisfied than with pure volumetric forcing, but at modest computational cost.

Since the effects of particle acceleration should be important during interparticle collisions and vortex entrainment, we apply a variable-density incompressible flow solver, *i.e.* the density ρ of the virtual fluid representing the particle phase is set equal to that of the solid. Tests reported in Truong et al. (2005a) showed that this approach does indeed predict particle acceleration better than when using a constant-density solver as done by previous workers.

The computations reported herein implement both volumetric and marker forcing, and additionally the hybrid of the two. We refer to the volumetric forcing of equation(3) as implemented with a variable-density solve, as the "VIV"method (Truong et al, 2005a). In marker forcing ("VIM"), an artificial forcing $\boldsymbol{F}(\boldsymbol{X}_m)$ is specified at marker locations $\boldsymbol{X}_m$ by:

$$\boldsymbol{F}(\boldsymbol{X}_m) = \rho_p h^3 \frac{(\boldsymbol{U}_p(\boldsymbol{X}_m) - \boldsymbol{U}(\boldsymbol{X}_m))}{\Delta t} \qquad (4)$$

where $\boldsymbol{U}(\boldsymbol{X}_m) = \sum \boldsymbol{u}\delta(\boldsymbol{X}_m - \boldsymbol{x})h^3$ is the fractional-step marker velocity, which is interpolated from nearby grid cells by Peskin's (2002) discretized Dirac delta function δ, and h is the grid spacing. The artificial body force $\boldsymbol{f}_p$ follows equation (5) below with α set to zero. Finally, in our hybrid method of volumetric and marker velocity-based forcing, called "VIV-VIM"(Truong et al, 2005b) the artificial body force $\boldsymbol{f}_p$ is specified as:

$$\boldsymbol{f}_p(\boldsymbol{x}) = \alpha\rho \frac{(\boldsymbol{u}_p - \boldsymbol{u})}{\Delta t} + \sum \delta(\boldsymbol{X}_m - \boldsymbol{x})\boldsymbol{F}(\boldsymbol{X}_m) \qquad (5)$$

Particle- particle interactions

To treat inter-particle contacts, and equivalently particle-wall contacts, we employ the "soft-sphere"Discrete Element Method (Tsuji et al. 1992), of which some details are provided on the next page. The coefficient of friction is taken to be 0.5 in the present simulations.

Marker forcing on solid and free boundaries

The rotating drum apparatus, which contains solid particles and possibly an interstitial liquid, is modeled as a cylindrical region embedded in a 3D Cartesian computational grid. In the dry case, denoted below by "air", the effect of fluid was ignored and the cylinder was represented in terms of its bounding surfaces when evaluating the contact forces with particles. For the liquid-immersed cases, the drum boundary is additionally represented, for the purpose of the flow calculation, as a set of discretized markers on the drum surface.

In the "open"drum configuration, a free surface is formed between liquid and air phases, and this is also represented computationally by a set of markers. We solve the fluid equations for the entire computational domain with variable density corresponding to the gas, liquid, and solid phases. The surface tension at the liquid-gas interface is then added to the momentum equation (1) (Tryggvason et. al, 2001).

Numerical Time-Stepping Scheme

A simple finite-volume method based on a staggered grid and central differences in space is employed to solve the variable density Navier-Stokes equations (Tryggvason et. al, 2001). Equation (1) is discretized from time level n to time level $n+1$ by a forward Euler method as:

$$\frac{\rho^{n+1}\boldsymbol{u}^{n+1} - \rho^n \boldsymbol{u}^n}{\Delta t} + \boldsymbol{A}^n = \boldsymbol{F}^n - \nabla\phi^{n+1} + \boldsymbol{f}^{n+1} \qquad (6)$$

whereΔt is the time step, ϕ^{n+1} is the pseudo-pressure,$A^n = \nabla_h \cdot \rho^n \boldsymbol{u}^n \boldsymbol{u}^n$ is the momentum advection term and $\boldsymbol{F}^n = \nabla_h \cdot \mu^n(\nabla_h \boldsymbol{u}^n + \nabla_h^T \boldsymbol{u}^n) - \nabla_h p^n + \rho^n \boldsymbol{g}$ is the intensive fluid force.

Substeps for the fluid ("F") phase, particle ("P") phase, and possibly the free surface ("S") and drum boundary "B"), are as follows:

P1) Update particle positions to the new t^{n+1}, detect particle contacts, and update particle velocity based on contact forces as modeled by springs and dashpots. Particles may enter and break contacts at a shorter time scale than that of the fluid flow. Thus, to step a particle from time t^n to t^{n+1}, we perform N (=5) substeps, indicated by k, which consist of the following tasks:

a) Advance particles from sub-step k to $k+1$ by

$$\boldsymbol{X}_p^{n+1,k+1} = \boldsymbol{X}_p^{n+1,k} + \Delta t\, \boldsymbol{U}_p^{n+1,k} \Big/ N \qquad (7)$$

b) Search for particle contacts, thereafter calculate the net contact force $\boldsymbol{F}_c^{n+1,k+1}$ and torque $\boldsymbol{T}_c^{n+1,k+1}$. For efficient contact search, we employ a cell-linked list method (Allen & Tildesley, 1987).

c) Calculate particle translational and angular velocities at substep k+1 as

$$\boldsymbol{U}_p^{n+1,k+1} = \boldsymbol{U}_p^{n+1,k} + \frac{\Delta t}{N}\frac{\boldsymbol{F}_c^{n+1,k+1}}{M_p} \tag{8}$$

$$\bar{\Omega}_p^{n+1,k+1} = \bar{\Omega}_p^{n+1,k} + \frac{\Delta t}{N}\frac{\boldsymbol{T}_c^{n+1,k+1}}{\boldsymbol{I}_p} \tag{9}$$

P2) Based on the updated particle velocity, calculate the added force and update the fluid velocity field, and then calculate the new density and viscosity fields ρ^{n+1} and μ^{n+1}.

S) Advect the free surface markers by local velocity interpolated at its location. Re-structure the connected markers by adding and/or deleting points and edge elements. Calculate the surface curvature and corresponding surface tension at the liquid-air interface, and add to the momentum equation.

F1)Calculate the momentum advection term $\boldsymbol{A}^n$ and the intensive fluid force $\bar{F}^n$ in each cell.

F2) Obtain the "fractional-step"momentum density $\rho^{n+1}\tilde{\boldsymbol{u}}$ by subtracting the advection term $\boldsymbol{A}^n$

$$\rho^{n+1}\tilde{\boldsymbol{u}} = \rho^n \boldsymbol{u}^n + \Delta t\,(\boldsymbol{F}^n - \boldsymbol{A}^n) \tag{10}$$

and thence the fractional step velocity $\tilde{\boldsymbol{u}}$.

F3) Project $\tilde{\boldsymbol{u}}$ onto a solenoidal velocity field by adding the gradient of a suitable pseudo-pressure.

P3)Within each particle, calculate the body force $\boldsymbol{f}_b$ by equation (3) and add to the fluid to yield a rigidified momentum density $\rho^{n+1}\boldsymbol{u}^{n+1}$

$$\rho^{n+1}\boldsymbol{u}^{n+1} = \rho^{n+1}\tilde{\boldsymbol{u}} + \Delta t \boldsymbol{f}_p^{n+1} \tag{11}$$

B) Impose the target velocity at the drum boundary by calculating the body force $\bar{f}_b$ and adding it to the fluid.

COMPARISON WITH ROTATING-DRUM EXPERIMENTS

This section briefly compares simulation results with experimental data from closed and open rotating drums, reported previously in Truong *et al* (2006, 2007a, 2007b). For the open drum, which has the additional complication of a free surface, only 2D simulations have been achieved.

Apparatus

Experiments were performed with air and sunflower oil as the interstitial fluids. We imaged the entire drum at 30 frames/sec with 1008x956 pixel resolution. Image analysis is done manually.

Closed Drum. 338 roughened glass spheres (ϕ12.5mm) occupied about half of the drum, whose internal diameter and width were respectively 179.4mm and 45.6mm. The front and rear walls are glass, while the outer wall is PMMA. Temperature of the air and oil was 25.5 $\pm$0.5°C, at which the density of the oil is 0.919 g/cm^3 and kinematic viscosity is 0.33 cm^2/s. Density of the beads is 2.49 g/cm^3.

Open Drum. Figure 1 is a photograph of the open-perimeter rotating drum. Two parallel circular PMMA plates are mounted on a steel axle with a separation between their inner surfaces of 22mm, and are sandwiched, with O-rings forming a seal, between front and rear vertical sidewalls of the flow tank. A wire mesh between the plates forms a circumference, of inner diameter 193.2mm, that confines glass beads while allowing oil to flow in and out of the drum chamber (left to right in the photo). Backflow under the drum is prevented by a plastic block machined to fit the wire mesh.

We report here on two runs; rotation rate and flow discharge are indicated in Table 1. The main difference between the two runs was the boundary conditions in the upstream and downstream tank; the first run had a horizontal plate set at the height of the cusp of the sealing block, while the level in the downstream tank was much lower in the second run than the first. 450 beads of diameter 6.0 mm, and 200 of diameter 5.0mm, were mixed to mitigate the formation of quasi-crystalline structure near the boundaries of the drum chamber. Temperature of the oil during experiments was 30.0 $\pm$0.5°C, for which density is 0.919 g/cm^3 and kinematic viscosity is 0.28 cm^2/s. Density of the beads is 2.440 g/cm^3.

Comparison

At the rather low rotation rates available with the closed-drum apparatus, beads avalanched intermittently, settling into rigid rotation between avalanches. Instantaneous slope of the bead surface was determined on the images immediately before avalanching, when the bed slope peaked, and when the slope reached a minimum as the avalanche lost strength. These bed angles are reported in Fig. 2, for oil and air, at 2 and 5 r.p.m. Agreement between simulation and experiment is very satisfactory. These data, together with time-averaged profiles of bead velocity (not shown) suggest that the oil only influenced the bead motion at the upper surface of the flowing layer.

Next, consider the results for the open drum given in Table 1. Note first that the results for bed angle, flow depth, and thickness of the flowing bead layer were very close for the two experimental cases, which suggests that the detailed flow conditions up- and downstream barely affect results. Comparing values from experiment *vs.* 2D simulation, overall agreement is seen to be satisfactory for the bed slope, but there is a significant discrepancy in the thickness of the flowing grain layer. Furthermore there is a factor of about two between the maximum bead velocities(not shown). The shape of the free surface was found to agree well between simulation and experiment. The differences may result from an "un-natural"resistance of simulated 2D granular assemblies to local deformation; shearing particles are forced to go over the tops of their neighbors, and the concomitant flow of liquid between pores is resisted by the narrow interparticle gaps. Thus 3D simulations are desired. However, their very high computational cost led us to proceed to 3D simulations in a doubly-periodic "channel", as described in the next section.

QUASI-D.N.S. OF BEDLOAD TRANSPORT IN DOUBLY-PERIODIC DOMAINS

This section presents results from quasi-DNS of bedload transport in a doubly-periodic pressure-driven "channel"of height H, width H, and streamwise length $4H$, where H is set to 250 wall units based on the imposed pressure drop. A monolayer of spheres is fixed to the lower wall, while the upper boundary is a stress-free lid. Particle diameter d is fixed at $H/10$, *i.e.* 25 wall units, and with a mesh of 40×40×160, there are 4 grid points per diameter. 1500 free particles are placed in the domain, enough to create a deposit of four layers on the bottom. We set material properties to those of sand in water at 20°C; dimensional viscosity is 0.010 g/(cm-s), relative density s is 2.6, and gravitational acceleration is 981 cm/s^2. Six values of dimensional diameter, d = 0.020, 0.030,... 0.070 cm, were specified to yield the cases shown in

Table 2.

To evaluate the particle Reynolds number $d^+ = du_\tau/\nu$ and nondimensional shear stress ("Shields parameter") $\Theta \equiv \tau_0/((s\text{-}1)gd)$, we determine u_τ based on the maximal value τ_0 of fluid shear stress (time-averaged in horizontal planes) over all heights. As seen from Table 2, d^+ takes values around 15, *i.e.* particle diameter is equivalent to the height of the near-wall streamwise vortices that would occur over a flat wall. The lowest value of Θ, 0.06, is about twice the threshold of about 0.033 for particle motion, as determined from the standard Shields plot.

Figure 3 shows, for d = 0.06, 0.04cm, and 0.02 cm (Θ = 0.08, 0.21, 0.70), snapshots of particle position as viewed from the side, overplotted by time-averaged profiles of solid concentration and of mixture velocity. As expected, higher Shields' parameter leads to a thicker layer of mobilized sediment. For the two lower transport stages, *i.e.* d = 0.06, 0.04, behavior at the upper and lower boundaries appears to be as hoped. In particular, the loose particles adjacent to the fixed layer are themselves motionless, and the sediment bed can accordingly be termed "erodible". By contrast, the corresponding particles at the highest transport stage (d= 0.02 cm) have a slight creeping motion, and it is not clear whether this can still be qualified as an erodible bed. Also at the highest transport stage, the profile of sediment concentration clearly seems influenced by the upper boundary; in particular, a deeper channel would allow particles to be lifted up into suspension.

Total sediment flux, *i.e.* the flux through cross-stream planes, is plotted versus Θ in Fig. 4, together with the well-known semiempirical formulae of Meyer-Peter and Mueller (1948), and Einstein (1942). The agreement with the former appears very good. However, Wong and Parker (2006) convincingly argue, based on reanalysis of the orginal data, that the usual prefactor of 8 in the MPM formula should be 4. This correction would shift the MPM curve to nearly overlay the Einstein curve, about a factor of two below the DNS. This difference may result from a number of factors. First, the threshold value of Shields' parameter that appears in the MPM formula, 0.047, is suitable for hydraulically rough sediment. In view of the low particle Reynolds number, it could be adjusted to the Shields' curve value of about 0.033. Second, the empirical formulae are based on flume tests with angular sediment, which are less mobile than the spherical particles in the simulations. However it may be moot to focus on such physical effects here, because the present simulations are clearly under-resolved, with concomitant uncertainty on the sediment flux data. Figure 5 compares, for *d=0.05*cm, profiles from a grid refinement test at a resolution that is double the standard specification of four points per particle diameter, in a foreshortened domain of dimensions $H\times H\times H$, (*i.e.* one quarter the length of the standard runs). One observes about a 30% increase in sediment flux, *i.e.* the integral of CU, when resolution is doubled from $h=d/4$ to $h=d/8$.

Fig 5 also shows the profiles from the standard-sized domain with d=0.05 cm. Though we have just seen that the runs at $h=d/4$ are under-resolved, it is still of interest to consider the effect of domain length in the two runs at this resolution. In particular, the profiles of velocity are identical below $y=5d$, *i.e.* in the bedload layer, while diverging rapidly above. This shows that the mechanism of shear resistance is altered for $y > 5d$ in the foreshortened domain; the most likely explanation is that large-scale streamwise vortices are suppressed, along with the Reynolds stress that they generate in the "full domain". Whatever the cause, the near overlap for $y < 5d$ suggests that such changes do not influence the mean properties of the bedload layer, at least for this particle diameter. For reference, we note that the peak in Reynolds stress is found to occur around $y = 4.8d$; below this level, the particle-supported stress rapidly dominates.

Next, if we compare profiles from the two runs at different grid resolutions in the foreshortened domain, we see that the bedload layer shears more easily in the better resolved computation. It is possible that under-resolution in this two-phase layer decreases the "effective" permeability to liquid flow there, which would presumably increase the resistance to shearing of the liquid-solid mixture.

CONCLUSION

We claim that the present work is the first to achieve turbulence simulation of bedload transport at a sediment transport rate above incipient motion; indeed the run for d = 0.020 cm yields rather intense transport. Unfortunately the runs performed to date in the full domain are seriously under-resolved, and the appelation "quasi-DNS" will be disputed by some in the DNS community. We would suggest that this term is still fair for the present application as, we believe, the motions responsible for Reynolds stress, *i.e.* eddies whose cross-sectional scale are of the order of the particle diameter, have been reasonably resolved. Below the peak in Reynolds stress, the stress is borne by the particles, rather than by liquid viscosity, and the demands on resolution are accordingly less stringent than those that apply to the buffer layer over a plane wall. Of course, further grid-refinement studies and related cross-checks are required to strengthen this claim, and to quantify the remaining uncertainty from under-resolution of particle boundary layers and of interparticle lubrication layers, and from the interparticle contact models. Concerning the reliability of the soft-sphere technique and associated contact models, we assert that some overall measure of confidence is provided by the comparison with rotating drum experiments.

Acknowledgements. We are grateful for financial support from Ritsumeikan University, to Mr. H. Sugimoto for designing and assembling the open-drum apparatus, to Ms. A.T.V. Nguyen and Mr. T.D. Nguyen for extensive experimental support, and to Ms. T.B. Nguyen for help with final preparation of the manuscript. We acknowledge with thanks numerous discussions with Prof. S. Egashira and Dr. T. Itoh.

REFERENCES

Allen, M.P. & Tildesley, D. 1987 *Computer Simulation of Liquids*, Clarendon Press, Oxford

Drake, T.G. & Calantoni J. 2001 Discrete particle model for sheet flow on the near shore, *Journal of Geophysical Research - Oceans*, 106-C9, 19859-19868

Einstein, H.A., Formulas for the transportation of bedload, *Trans. Am. Soc. Civ. Eng.*, 107, 561-597, 1942.

Gotoh, H., Harada, E., Sakai, T. 2000 Movable bed simulator for fractional transport of graded sediment, *Annual J. Hydraulic Engineering, JSCE*, Vol. 44, 665-670

Kajishima, T. & Takiguchi, S. 2002 Interaction between particle clusters and particle-induced turbulence, *Int.J. Heat Fluid Flow* 23, 639-646

Meyer-Peter, E., and R. Muller, Formulas for bed-load transport, in *Proceedings of the* 2^{nd} *Meeting of the International Association for Hydraulic Structures Research*, pp. 39-64, Inter. Assoc. for Hydraul. Res., Delft, Netherlands,

1948.

Peskin, C.S. 2002 The immersed boundary method, *Acta numerica*, 11:479-517

Schmeeckle, M. W. 1998 *The Mechanics of Bedload Sediment Transport*: Ph.D. dissertation, Univ. of Colorado.

Truong, J.C. Wells, A.T.V. Nguyen 2007a Development of Fictitious-Domain Simulations of Erodible Particle Beds in *Proc. River, Coastal, and Estuarine Morphodynamics (RCEM)*, Twente, Netherlands, Sept. 2007.

Truong, H. V., Nguyen, A., Sugimoto, H., Wells, J.C. 2007b Fictitious domain simulations of bedload transport, free-surface flow in a rotating tumbler. *JSCE Annual J. Hydraulic Engineering*. 51,CD-ROM

Truong, H. V., Wells, J.C., Nguyen, A. 2006 An experimental check on particle dynamics simulations of erodible particle beds; the rotating tumbler. *JSCE Annual J. Hydraulic Engineering*. 50, CD-ROM

Truong, H.V., Wells, J.C., Tryggvason, G. 2005a: Explicit vs. implicit particle-liquid coupling in fixed-grid computations at moderate particle Reynolds number, FEDSM2005-77206, *Proc. ASME FED Summer Meeting*, Houston TX

Truong, H.V., Wells, J.C., Tryggvason, G. 2005b Implicitly - coupled finite difference schemes for fictitious domain simulation of solid-liquid flow; marker, volumetric, and hybrid forcing, *Proc. ERCOFTAC workshop, DLES VI* Sept.,2005, Poitiers France. Springer

Tsuji, Y., Tanaka, T., Ishida, T. 1992 Lagrangian numerical simulation of plug flow of cohesionless particles in horizontal pipe, *Powder Technology* 71: 239-250

Tryggvason, G., Brunner, B., Esmaeeli, A., Juric, D., Alrawashi, N., Tauber, W., Han, J., Nas, S., Jan, Y.J. 2001 A front-tracking method for the computation of multiphase flow, *J. Comput. Phys.*, 169:708-759

Uhlmann, M. Direct numerical simulation of sediment transport in a horizontal channel. Technical Report No. 1088, CIEMAT, Madrid, Spain, 2006. ISSN 1135-9420.

Uhlmann, M. An immersed boundary method with direct forcing for the simulation of particulate flows, 2005. *J. Comput. Phys.*, 209:448-476

Wong M. Parker G. 2006. The bedload transport relation of Meyer-Peter and Muller overpredicts by a factor of two. *Journal of Hydraulic Engineering* 132(11): 1159-1168.

Werner, B.T., Haff, P.K., 1988 The impact process in aeolian saltation: Two-dimensional simulations, *Sedimentology*, 35:189-19.

Table 1: Conditions for two matched runs in the open drum, with up- and downstream boundary conditions changed somewhat as described in the text, and the resulting bed angle, clear-liquid flow depth h_t, and thickness t of the flowing grain layer. Parenthetical values are results from 2D simulations.

Specific Discharge q_f (cm^2/s)	Rotation Rate Ω(rpm)	Bed Angle θ(degree)	h_t/d	t/d
31.2	6.17	16.9	0.50	2.56
31.3	6.15	16.4 (18.4)	0.52 (0.90)	2.36 (3.62)

Table 2: Parameters for quasi-DNS of bedload transport, and in doubly-periodic channel.

Particle diameter d(cm)	Particle Reynolds numbers Re_d	Shields parameter Θ	Dimensionless Bedload Trasport rate Q_s
0.07	18.6	0.06	0.010
0.06	17.1	0.08	0.014
0.05	16.0	0.13	0.030
0.04	14.4	0.21	0.058
0.03	12.7	0.38	0.094
0.02	9.40	0.70	0.151

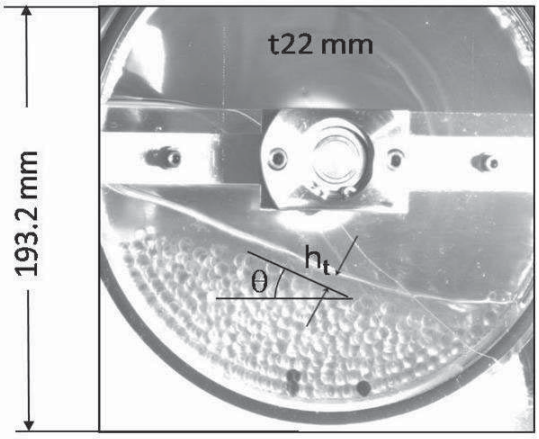

Figure 1: Photograph of the "open"drum during the run on the second line of Table 1. Drum rotation is clockwise; oil flow is left to right. Three black tracer particles are visible. Bed angle ϕ and liquid flow thickness h_t, tabulated in Table 1, are indicated. Some 70% of the beads are ϕ6, the remainder ϕ5.

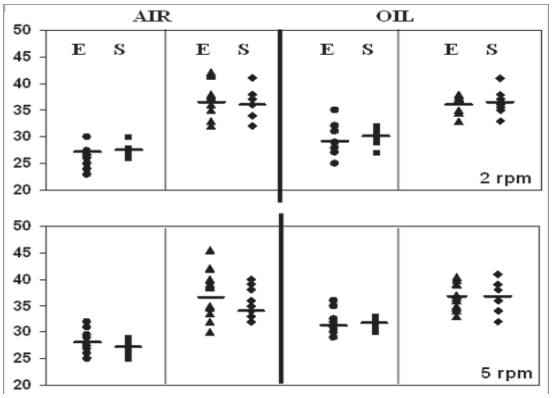

Figure 2: Closed drum; comparisons between (E)xperiment and (S)imulation of the temporal maximal and minimal bed angles for 2 and 5r.p.m. rotation speeds, in air and oil.

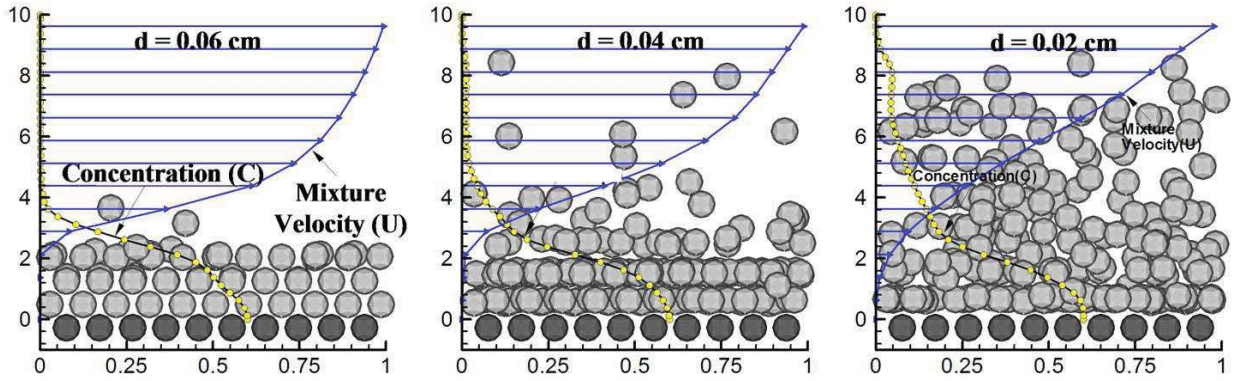

Figure 3: Snapshots of particle positions, with temporally-averaged profiles of solid concentration and mixture velocity, for d = 0.06, 0.04, and 0.02 cm (Θ= 0.08, 0.21, 0.70) respectively.

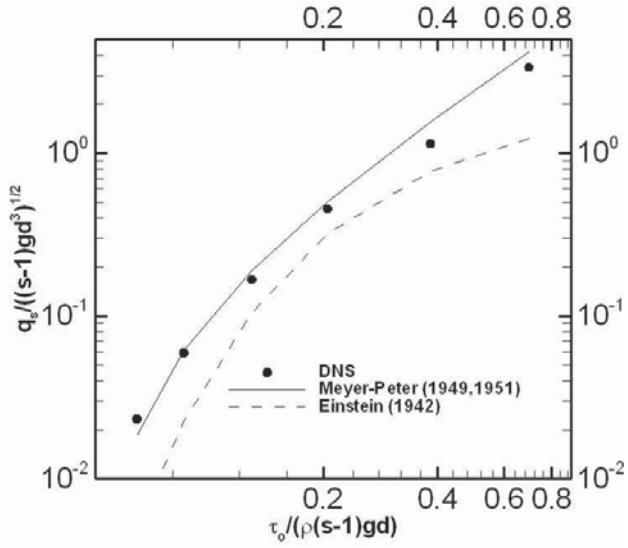

Figure 4: Comparison of nondimensional bedload flux from present simulation ("DNS"in legend) with empirical correlations.

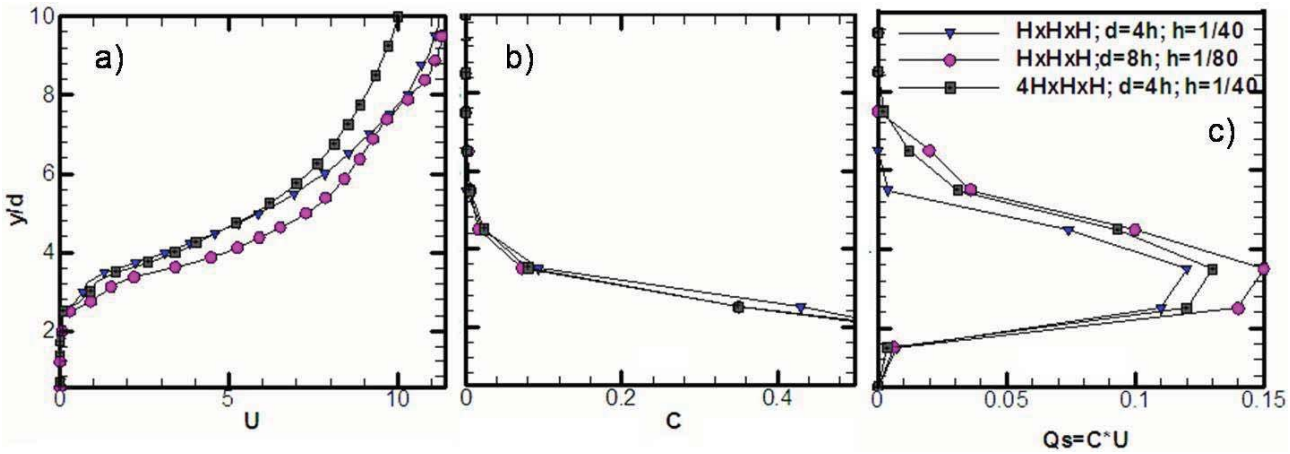

Figure 5: Effect of channel size ($H\times H\times H$ vs $4H\times H\times H$, as specified by legend in c) and resolution (d=4h *vs.* d=8h) for d=0.05 cm. Profiles of: a) mixture velocity U (nondimensionalized by friction velocity), b) particle volume fraction C, c) sediment flux intensity CU .